Journal of Coordination Chemistry

ISSN: 0095-8972 (Print) 1029-0389 (Online) Journal homepage: http://www.tandfonline.com/loi/gcoo20

Synthesis, structure, and spectroscopic properties of Cu^{+} complexes and its application to solar cells

Ting-Hong Huang, Jie Yan, Hu Yang, Huai-Ming Du & Min-Hua Zhang

To cite this article: Ting-Hong Huang, Jie Yan, Hu Yang, Huai-Ming Du & Min-Hua Zhang (2015) Synthesis, structure, and spectroscopic properties of Cu^{+} complexes and its application to solar cells, Journal of Coordination Chemistry, 68:9, 1514-1527, DOI: 10.1080/00958972.2015.1025770

To link to this article: http://dx.doi.org/10.1080/00958972.2015.1025770

Accepted author version posted online: 04 Mar 2015.
Published online: 27 Mar 2015.

Journal of Coordination Chemistry, 2015
Vol. 68, No. 9, 1514–1527, http://dx.doi.org/10.1080/00958972.2015.1025770

Synthesis, structure, and spectroscopic properties of Cu^+ complexes and its application to solar cells

TING-HONG HUANG*†, JIE YAN†, HU YANG†, HUAI-MING DU† and MIN-HUA ZHANG‡

†Key Laboratories of Fine Chemicals and Surfactants in Sichuan Provincial Universities, Material Corrosion and Protection Key Laboratory of Sichuan Province, College of Materials and Chemical Engineering, Sichuan University of Science & Engineering, Zigong, China
‡Key Laboratory for Green Chemical Technology (Ministry of Education of China), R&D Center for Petrochemical Technology, Tianjin University, Tianjin, China

(*Received 1 September 2014; accepted 23 February 2015*)

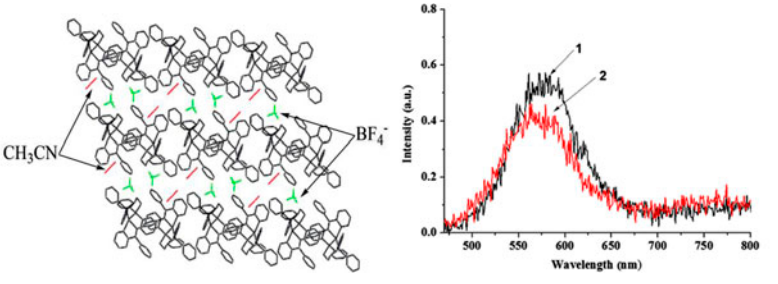

A series of Cu^+ complexes, $[Cu_2(L)(dppe)_2](BF_4)_2$ (**1**), $[Cu_2(L)(dppp)_2](BF_4)_2{\cdot}2CH_3CN$ (**2**), and $[Cu_2(L)(dppe)_2](ClO_4)_2$ (**3**) (L = N,N′-bis(dipyridin-2-ylmethylene)benzene-1,4-diamine, dppe = 1,2-bis(diphenylphosphino)ethane, and dppp = 1,3-bis(diphenyl phosphino)propane), have been synthesized and characterized by IR, ^1H NMR, ^{31}P NMR, UV–vis spectrum, and X-ray crystal structure analysis. The structural analysis reveals each Cu^+ is four-coordinate N_2P_2 and adopts a distorted-tetrahedral geometry. Crystal structures of **1–3** contain 1-D supramolecular arrays constructed by intermolecular $\pi\cdots\pi$ interactions, with variations in π-stacking patterns. The ordered-layer-lattice BF_4^- or CH_3CN is located between 1-D arrays. The absorption peaks of **1** and **2** in acetonitrile at room temperature display ILCT and MLCT absorptions. Emission experiments show solid-state emissions of **1** and **2** are not similar to those of solution samples. The conversion efficiency of **1** and **2** in dye-sensitized solar cells is extremely poor (<0.1%).

Keywords: Copper(I) complexes; Crystal structures; Spectra; DSSC

1. Introduction

Copper(I) complexes are under active investigation as alternatives to Ru(II) complexes for its photophysical properties [1–5] and photoelectrochemical applications, such as light-emitting

*Corresponding author. Email: hth_chem@126.com

electrochemical cells [6] and dye-sensitized solar cells (DSSC) [7–10], especially due to their low toxicity and the high abundance of copper in comparison with similar transition metals [11]. Cu(I) complexes with multi-pyridyl ligands are of particular interest due to the numerous photophysical similarities they share with archetypal $[Ru(bpy)_3]^{2+}$ salts (bpy = 2,2′-bipyridine) [12]. The main difference between d^{10} Cu(I) compounds and low-spin d^6 Ru(II) compounds lies in the anticipated uncertainty of the former [7]. However, it is surprising that, to the best of our knowledge, DSSC with copper(I) dyes reported are relatively rare [13–17]. One of the key factors may be air-stable copper(I) complexes with multi-pyridyl ligands being hard to synthesize. As mentioned previously [18–21], bulky phosphine groups effectively prevent the geometric relaxation of the excited state. So some diverse phosphine ligands were generated to construct polymers [22–25] or supramolecular structures [26, 27] by self-assembly, and to pursue highly efficient luminescent complexes [28–32]. Much attention has been paid to the design and construction of $[Cu(NN)(PP)]^+$ system by changing the organic phosphine ligands coordinated to metal centers [33–35]. Currently, $[Cu(NN)(PP)]^+$ is of growing interest for supramolecular structures by metallo-subunits [36], but predicting and designing them are difficult because of the weakness of interactions involved. In particular, intermolecular C–H$\cdots\pi$ and $\pi\cdots\pi$ stacking interactions have led to unusual packing structures and spectroscopic properties [37–39].

Herein, we report the synthesis, structure, and spectroscopic properties of three copper(I) complexes, $[Cu_2(L)(dppe)_2](BF_4)_2$ (**1**), $[Cu_2(L)(dppp)_2](BF_4)_2$ (**2**), and $[Cu_2(L)(dppe)_2](ClO_4)_2$ (**3**) (dppe = 1,2-bis(diphenylphosphino)ethane, dppp = 1,3-bis(diphenylphosphino) propane, and L = N,N′-bis(dipyridin-2-ylmethylene)benzene-1,4-diamine). Intermolecular π-stacking interactions lead to construction of 1-D supramolecular arrays and the ordered-layer-lattice anions (BF_4^- in **1** and **3**, BF_4^- and CH_3CN in **2**) are located between these arrays. The absorption, emission, and excitation spectra of **1** and **2** have been investigated at room temperature. Complexes **1** and **2** as sensitizers in DSSC were also observed.

2. Experimental

2.1. *General methods and materials*

All chemicals were of A.R. grade and were used as received without purification. N,N′-bis (dipyridin-2-ylmethylene)benzene-1,4-diamine (L) was prepared according to the literature [40–42]. IR spectra were recorded as KBr pellets on a Nicolet 6700 spectrometer from 4000 to 450 cm^{-1}. ^1H and $^{31}P\{^1H\}$ spectra were recorded on a Bruker instrument at 400.15 and 161.98 MHz, respectively. Absorption spectra of **1** and **2** in acetonitrile were measured with a Varian CARY-50UV spectrophotometer. The luminescence spectra of **1** and **2** in acetonitrile were measured at room temperature on a Cary Eclipse fluorescence spectrophotometer. Solid-state luminescence spectra of **1** and **2** were measured on a FL3-P-TCSPC fluorescence spectrophotometer. The DSSC were carried out on a 100 $mWcm^{-2}$ AM 1.5 simulated sunlight and the system had been calibrated with a standard single-crystal Si photovoltaic cell. The current–voltage (*I–V*) characteristics of the cells were measured using a Keithley 2400 source meter.

CAUTION! Perchlorate salts are potentially explosive and should be synthesized in small quantities and handled with great care.

2.2. *Preparation of $[Cu_2(L)(dppe)_2](BF_4)_2$ (1)*

A mixture of $[Cu(CH_3CN)_4]BF_4$ (0.0158 g, 0.050 mmol) and dppe (0.0199 g, 0.050 mmol) in 4 mL CH_3CN was stirred at room temperature for 0.5 h and then L (0.0110 g, 0.025 mmol) was added. The reaction mixture was stirred for 0.5 h at room temperature. Vapor diffusion of diethyl ether into the solution gave red block crystals. The complex was obtained by filtration, washed with diethyl ether, and dried *in vacuo*. Yield: 0.0134 g (35%).

IR (cm^{-1}): 3052(m), 1586(w), 1486(w), 1434(m), 1329(w), 1089(s), 1055(vs), 847(w), 748(m), 696(m), 518(m). ^1H NMR (400 MHz, CD_3SOCD_3, 25 °C, TMS): δ = 2.20–2.48 (8H, P–CH_2–), 7.20–7.45 (44H, N–C_6H_4–N + PPh_2), 7.60–8.25 (16H, bipy). $^{31}P\{^1H\}$ NMR (CD_3SOCD_3, 25 °C, TMS): −3.45 ppm.

2.3. *Preparation of $[Cu_2(L)(dppp)_2](BF_4)_2 \cdot 2CH_3CN$ (2)*

A mixture of $[Cu(CH_3CN)_4]BF_4$ (0.0158 g, 0.050 mmol) and dppp (0.0206 g, 0.050 mmol) in 4 mL CH_3CN was stirred at room temperature for 0.5 h and then L (0.0110 g, 0.025 mmol) was added. The reaction mixture was stirred for 0.5 h at room temperature. Vapor diffusion of diethyl ether into the solution gave red block crystals. The complex was obtained by filtration, washed with diethyl ether, and dried *in vacuo*. Yield: 0.0178 g (46%).

IR (cm^{-1}): 3059(w), 2937(w), 2251(w), 1613(m), 1481(m), 1434(s), 1328(s), 1060(vs), 850(w), 748(s), 698(s), 513(m). ^1H NMR (400 MHz, CD_3SOCD_3, 25 °C, TMS): δ = 2.49–2.51 (12H, P–CH_2– + –CH_2–), 7.12–8.71 (60H, N–C_6H_4–N + PPh_2 + bipy). $^{31}P\{^1H\}$ NMR (CD_3SOCD_3, 25 °C, TMS): −12.82 ppm.

2.4. *Preparation of $[Cu_2(L)(dppe)_2](ClO_4)_2$ (3)*

A mixture of $[Cu(CH_3CN)_4]ClO_4$ (0.0163 g, 0.050 mmol) and dppe (0.0199 g, 0.050 mmol) in 4 mL CH_3CN was stirred at room temperature for 0.5 h and then L (0.0110 g, 0.025 mmol) was added. The reaction mixture was stirred for 0.5 h at room temperature. Vapor diffusion of diethyl ether into the solution gave red block crystals. The complex was obtained by filtration, washed with diethyl ether, and dried *in vacuo*. Yield: 0.0058 g (15%).

IR (cm^{-1}): 3074(w), 1613(w), 1585(w), 1492(w), 1433(s), 1330(m), 1091(vs), 847(w), 747(s), 695(s), 621(w), 517(m). ^1H NMR (400 MHz, CD_3SOCD_3, 25 °C, TMS): δ = 2.45–2.56 (8H, P–CH_2–), 7.27–7.74 (44H, N–C_6H_4–N + PPh_2), 7.79–8.47 (16H, bipy).

2.5. *X-ray crystallography*

Crystals suitable for X-ray structure analysis were obtained by vapor diffusion of diethyl ether into a solution of **1–3** in acetonitrile. Reflection intensity data were collected on a Bruker APEX CCD diffractometer with graphite-monochromated Mo-Kα radiation (λ = 0.71073 Å) using the ω technique at room temperature. All structures were solved by direct methods and refined by full-matrix least-squares on all F^2 data using SHELXTL. All hydrogens were generated geometrically, assigned fixed isotropic thermal parameters, and included in structure factor calculations. Crystal and structure refinement data are summarized in table 1. Selected bond lengths and angles are given in table 2.

Table 1. Crystal data and structure refinement details of **1–3**.

Complex	**1**	**2**	**3**
Empirical formula	$C_{80}H_{68}B_2Cu_2F_8N_6P_4$	$C_{86}H_{78}B_2Cu_2F_8N_8P_4$	$C_{80}H_{68}Cl_2Cu_2\ N_6O_8P_4$
Formula weight	1537.98	1648.14	1563.26
Crystal system	Monoclinic	Triclinic	Monoclinic
Space group	P2(1)/*n*	P-1	P2(1)/*n*
a (Å)	14.1312(10)	13.0111(12)	14.2581(8)
b (Å)	12.0855(9)	13.9468(13)	12.1332(7)
c (Å)	21.9965(16)	14.0130(11)	21.9482(14)
α (°)	90	119.777(5)	90
β (°)	98.034(5)	96.721(6)	99.296(4)
γ (°)	90	107.285(6)	90
Volume (Å^3), *Z*	3719.7(5), 2	1997.1(3), 1	3747.1(4), 2
ρ_{calc} (g cm^{-3})	1.373	1.370	1.386
μ (mm^{-1})	0.726	0.682	0.784
F(0 0 0)	1580	850	1612
θ range (°)	1.87–25.00	1.73–25.00	1.85–25.00
Reflections collected	28,282	15,444	28,194
Independent reflections	6545 [*R*(int) = 0.1053]	6935 [*R*(int) = 0.0263]	6589 [*R*(int) = 0.0367]
Data/restraints/parameters	4582/0/316	6935/0/497	6589/0/460
Goodness-of-fit on F^2	1.013	1.066	1.077
Final *R* indices [$I > 2\sigma(I)$]	$R_1 = 0.0675$	$R_1 = 0.0471$	$R_1 = 0.0640$
	$wR_2 = 0.1543$	$wR_2 = 0.1316$	$wR_2 = 0.1864$
R indices (all data)	$R_1 = 0.1480$	$R_1 = 0.0655$	$R_1 = 0.0881$
	$wR_2 = 0.1781$	$wR_2 = 0.1411$	$wR_2 = 0.2034$
Largest diff. peak and hole (e Å^{-3})	0.834 and −0.547	0.588 and −0.510	1.016 and −0.522

Table 2. Selected bond lengths (Å) and angles (°) for **1–3**.

1	
Cu(1)–N(1) 2.037(4)	N(1)–Cu(1)–N(3) 80.35(16)
Cu(1)–N(3) 2.051(4)	N(1)–Cu(1)–P(2) 126.07(12)
Cu(1)–P(2) 2.2507(18)	N(3)–Cu(1)–P(2) 116.61(12)
Cu(1)–P(1) 2.2574(16)	N(1)–Cu(1)–P(1) 130.03(12)
	N(3)–Cu(1)–P(1) 114.78(12)
	P(2)–Cu(1)–P(1) 90.92(6)
2	
Cu(1)–N(1) 2.033(2)	N(1)–Cu(1)–N(2) 79.24(9)
Cu(1)–N(2) 2.103(2)	N(1)–Cu(1)–P(1) 134.58(7)
Cu(1)–P(1) 2.2186(8)	N(2)–Cu(1)–P(1) 109.34(7)
Cu(1)–P(2) 2.2471(9)	N(1)–Cu(1)–P(2) 117.15(7)
	N(2)–Cu(1)–P(2) 103.85(7)
	P(1)–Cu(1)–P(2) 104.21(3)
3	
Cu(1)–N(1) 2.036(3)	N(1)–Cu(1)–N(2) 79.94(12)
Cu(1)–N(2) 2.061(3)	N(1)–Cu(1)–P(2) 127.32(10)
Cu(1)–P(2) 2.2518(13)	N(2)–Cu(1)–P(2) 117.12(9)
Cu(1)–P(1) 2.2564(12)	N(1)–Cu(1)–P(1) 129.31(9)
	N(2)–Cu(1)–P(1) 114.07(9)
	P(2)–Cu(1)–P(1) 90.88(5)

2.6. *Computational details*

The quantum chemical calculations for **1** and **2** were carried out with LDA-DFT as implemented in the Dmol^3 package provided by Materials Studio. The local functional for the exchange correlation potential is LDA-PWC. The core electrons for metals were treated by

effective core potentials. Self-consistent field density convergence was 10^{-4}. The basis set is DND. The convergence tolerances for energy change, maximum force, and maximum displacement between optimization cycles were set as 1.0×10^{-4} Ha, 0.02 Ha Å^{-1}, and 0.05 Å, respectively.

3. Results and discussion

3.1. *Syntheses*

The reaction of copper(I) salt with phosphine ligands (dppe or dppp) and L in a ratio of 2 : 2 : 1 at room temperature afforded dinuclear Cu(I) complexes **1–3**. At room temperature, **1** and **2** are soluble in DMF, DMSO, CH_3COCH_3, CH_3CN, and CH_2Cl_2, slightly soluble in $CHCl_3$, and hardly soluble in toluene.

IR spectra for **1**, **2,** and **3** mainly reflect the binding patterns of dppe, dppp, ClO_4^-, and BF_4^-. The strong peaks near 1434 cm^{-1} are $\upsilon_{Ph(P-Ph)}$, in agreement with complexes containing dppe or dppp. The strong peaks at 1055–1060 cm^{-1} are B–F stretches of BF_4^-, while the peak at 1090 is assigned to Cl–O stretches of ClO_4^-. The absorption peaks at 1480–1490 cm^{-1}, 850–690 cm^{-1}, and near 517 cm^{-1} are δ_{C-CH} (in the plane), δ_{C-C} (in and out the plane), and $\upsilon_{Cu-P,}$ respectively. In **2**, the absorption at 2251 cm^{-1} is attributed to $\upsilon_{(C\equiv N)}$. The absorption peak near 1586 cm^{-1} is $\upsilon_{(C=N)}$ of **1–3**. The ^{1}H NMR spectra of **1** and **3** show expected resonances typical for coordinated dppe, dppp, and L. In the ^{31}P NMR spectra of **1** and **2** singlets at −3.45 and −12.82 ppm indicate their electronic environments are different and this is reflected in the different chemical shifts observed in figure 1.

3.2. *Crystal structures*

The molecular structures of **1–3** were established using X-ray diffraction. Crystallographic data for the complexes are provided in table 1. Selected bond lengths and angles are in table 2. Structural analysis displays that intermolecular π–π stacking interactions lead to formation of 1-D supramolecular arrays with different types of π-stacking patterns.

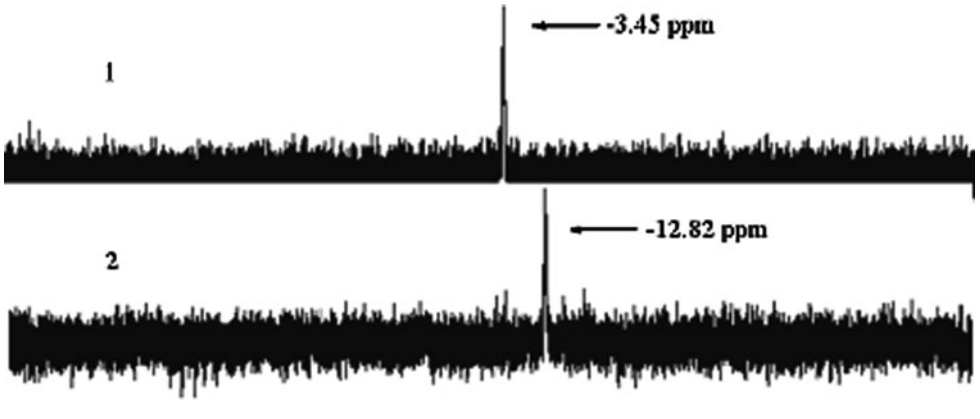

Figure 1. The ^{31}P NMR spectra of **1** and **2**.

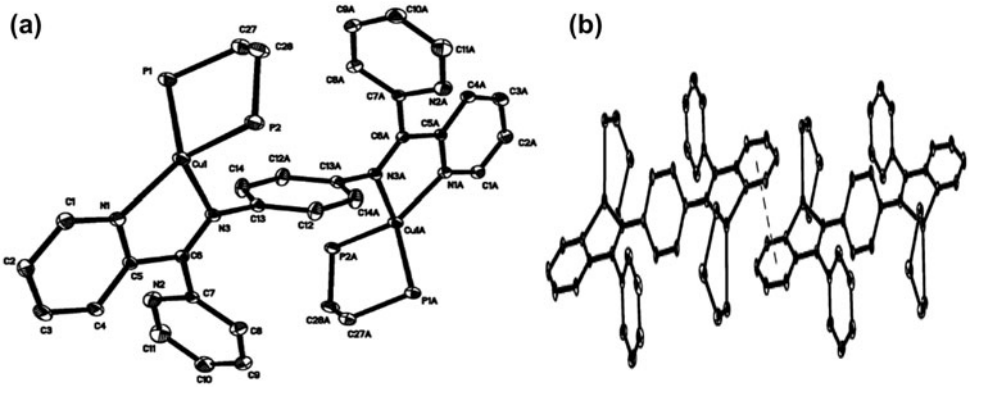

Figure 2. (a) Cation structure of **1**. The hydrogens and phenyl rings of dppe are deleted for clarity. (b) Intermolecular $\pi\cdots\pi$ stacking interactions between two molecules. The hydrogens are deleted for clarity.

3.2.1. Crystal structure of $[Cu_2(L)(dppe)_2](BF_4)_2$ (1). X-ray diffraction analysis for **1** reveals that the asymmetric unit contains half a L, one Cu^+, one dppe, and one BF_4^-. As shown in figure 2(a), the labile L is in a *trans* coordination mode to bridge two Cu ions, each of which possesses a distorted tetrahedral geometry with coordination of two N from L and two P from dppe. The bond distances of Cu–N [2.037(4) and 2.051(4) Å] and Cu–P [2.2507(18) and 2.2574(16) Å] are within the normal ranges [43]. Corresponding N–Cu–N and P–Cu–P bond angles are 80.35(16)° and 90.92(6)°, N–Cu–P bond angles change from 114.78(12)° to 130.03(12)° and the metal ions are separated by a Cu(I)···Cu (I) distance of 8.54 Å. Intramolecular edge-face (C–H$\cdots\pi$) interactions are observed from the edge of one phenyl (C12) to the face of another phenyl ring (C29–C30–C31–C32–C33–C34) attached to phosphorus (centroid-to-centroid distance: 4.661 Å, dihedral angle: 47.69° and H$\cdots\pi_{centroid}$: 2.78 Å).

In the solid state, intermolecular $\pi\cdots\pi$ stacking interactions are incorporated into 1-D tape-like arrays along the *a* axis [figure 2(b)]. The neighboring pyridyl rings from different dinuclear cations $[Cu_2(L)(dppe)_2]^{2+}$ are parallel to each other with a centroid-to-centroid distance of 3.586 Å and a dihedral angle of 0°, displaying the existence of significant $\pi\cdots\pi$ stacking interactions [figure 2(b)]. The intermolecular C–H$\cdots\pi$ interactions between phenyl rings attached to phosphorus with centroid-to-centroid distances of 4.986 and 4.958 Å, dihedral angles of 84.08° and 84.11° and H$\cdots\pi_{centroid}$ distances of 2.86 and 2.69 Å are

Table 3. Hydrogen-bond geometry of **1** (Å, °).

D–H···*A*	*D*–H	H···*A*	*D*···*A*	*D*–H···*A*
C(2)–H(2)···F(4)^{i}	0.93	2.49	3.19	133
C(10)–H(10)···F(3)^{ii}	0.93	2.53	3.41	160
C(31)–H(31)···F(3)^{iii}	0.93	2.45	3.26	146
C(12)–H(12)···Cg1	0.93	2.78	3.48	133
C(11)–H(11)···Cg1^{iv}	0.93	2.86	3.73	156
C(22)–H(22)···Cg2^{v}	0.93	2.69	3.62	171

Symmetry codes: (i) $1/2-x$, $1/2+y$, $1/2-z$; (ii) $1-x$, $1-y$, $-z$; (iii) $1-x$, $-y$, $-z$; (iv) x, $1+y$, z; (v) $3/2-x$, $-1/2+y$, $1/2-z$. The Cg1 and Cg2 are the centroids of the C21–C26 and N1–C1–C2–C3–C4–C5 rings, respectively.

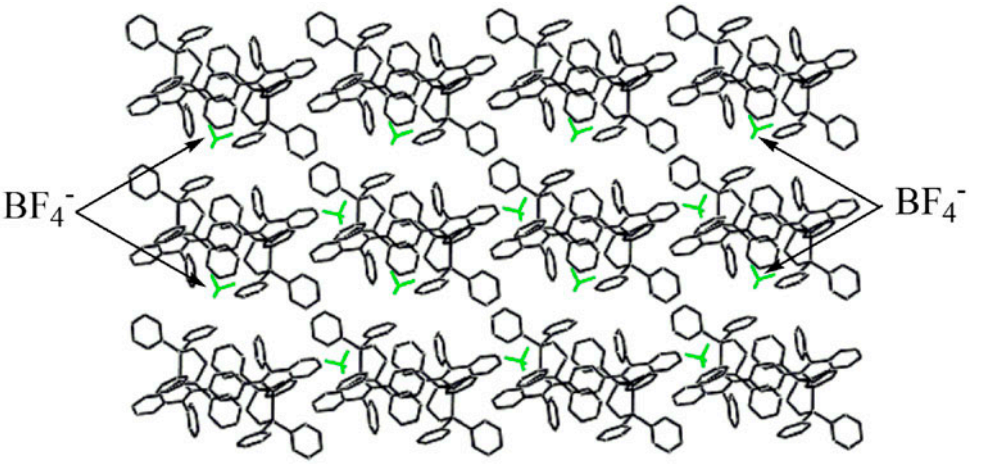

Figure 3. The 1-D tape-like arrays of $[Cu_2(L)(dppe)_2]^{2+}$ (black) separated by the ordered-layer-lattice (green) in **1** (see http://dx.doi.org/10.1080/00958972.2015.1025770 for color version).

observed as molecules extend to generate a 2-D network (table 3). All these reveal that the 2-D network is controlled by intermolecular $\pi\cdots\pi$ and C–H$\cdots\pi$ interactions. The ordered-layer-lattice BF_4^- is located between 1-D tape-like arrays [figure 3]. In the packing structure, weak interactions of C–H$\cdots$F hydrogen bonds are also observed in table 3.

3.2.2. Crystal structure of $[Cu_2(L)(dppp)_2](BF_4)_2\cdot 2CH_3CN$ (2). For **2**, the overall structure formed is analogous to that of **1**, having a discrete linear dinuclear centrosymmetric structure [figure 4(a)]. The inversion center is located at the center of phenylene. The labile L in a *trans* coordination mode links two Cu^+ ions, each of which adopts a distorted tetrahedral geometry constructed by two P from dppp and two N from L. The bond distances of Cu–P vary from 2.2186(8) to 2.2471(9) Å and the average distance of Cu–N is 2.068 Å, comparable with those in similar complexes [43–45]. The N–Cu–N and P–Cu–P bond angles are

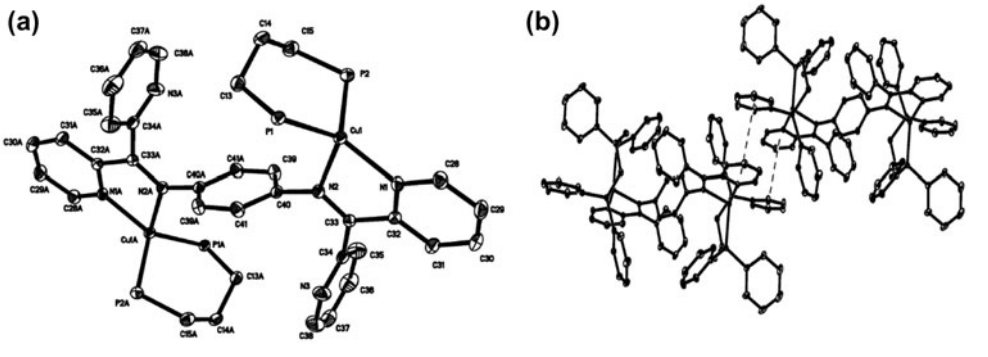

Figure 4. (a) Cation structure of **2**. (b) Intermolecular $\pi\cdots\pi$ stacking interactions between two molecules. The hydrogens and phenyl rings of dppp are deleted for clarity.

79.24(9)° and 104.21(3)°, N–Cu–P bond angles change from 103.85(7) to 134.58(7)° and the Cu(I)···Cu(I) distance of 8.70 Å is larger than the corresponding values in **1**. Similar intramolecular edge-face (C–H···π) interactions are observed with centroid-to-centroid distances of 5.152 and 5.071 Å, dihedral angles of 59.24° and 77.63° and H···$\pi_{centroid}$: 2.92 and 2.98 Å.

In the solid state, intermolecular π···π stacking interactions are incorporated into 1-D supramolecular arrays along the *b* axis, which shows π-stacking in **2** is much different from **1** [figure 4(b)]; the BF_4^- and CH_3CN are located between the chains [figure 5]. The planes between one phenylene ring of PPh_3 and the pyridyl ring of a neighboring molecule are approximately parallel with mean interplanar separation of 3.73 Å, a little longer than those in **1**, and a dihedral angle of 10.75° [figure 4(b)]. Moreover, the supramolecular arrays of $[Cu_2(L)(dppp)_2]^{2+}$ are separated in the ordered-layer-lattice by CH_3CN and BF_4^- in **2** [figure 5]. However, intermolecular C–H···π interactions are not observed because of the influence of the methylene. The structure also involves weak interactions of C–H···F and C–H···N hydrogen bonds between the cations in the packing structure (table 4).

3.2.3. Crystal structure of $[Cu_2(L)(dppe)_2]$ $(ClO_4)_2$ (3). The overall structure of **3** is analogous to that of **1**, which is due to ClO_4^- instead of BF_4^- in the reaction [figure 6]. However, the interplanar distance between pyridyl rings from anions $[Cu_2(L)(dppe)_2]^{2+}$ is ca. 3.60 Å, a little longer than those in **1**, and the short distances of atom/atom are 3.407 Å [figure 6(a)]. In addition, similar C–H···π interactions and weak interactions of C–H···O hydrogen bonds in the packing structure are observed (table 5).

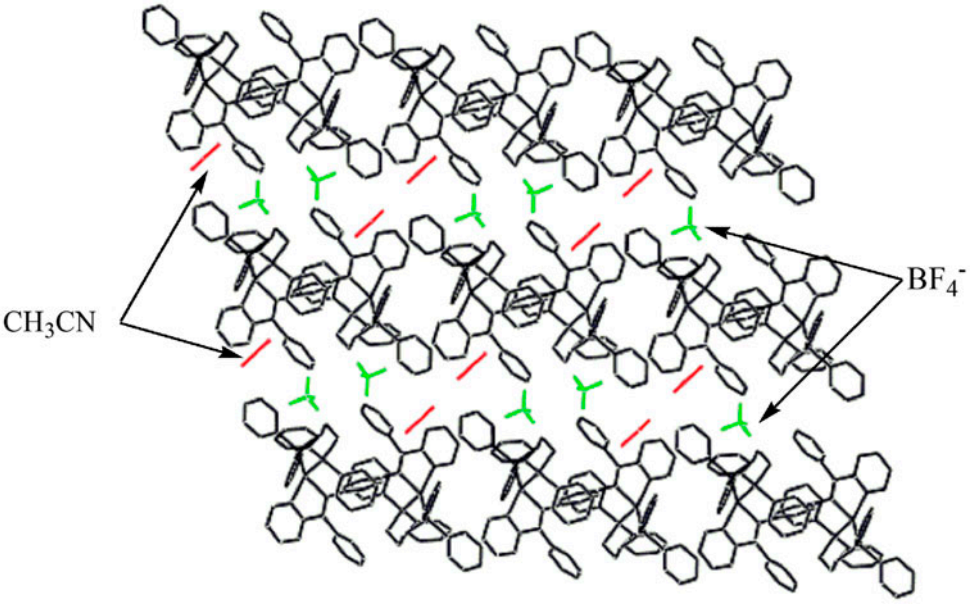

Figure 5. The 1-D tape-like arrays of $[Cu_2(L)(dppp)_2]^{2+}$ (black) separated by the ordered-layer-lattice (green) and CH_3CN (red) in **2** (see http://dx.doi.org/10.1080/00958972.2015.1025770 for color version).

Table 4. Hydrogen-bond geometry of **2** (Å, °).

D–H···*A*	*D*–H	H···*A*	*D*···*A*	*D*–H···*A*
C(8)–H(8)···F(1)	0.93	2.53	3.39	154
C(10)–H(10)···F(2)^{i}	0.93	2.49	3.37	159
C(30)–H(30)···N(4)^{ii}	0.93	2.56	3.49	177
C(36)–H(36)···F(1)^{iii}	0.93	2.47	3.30	150

Symmetry codes: (i) $1-x, 1-y, 2-z$; (ii) $1+x, y, z$; (iii) $1-x, -y, 1-z$.

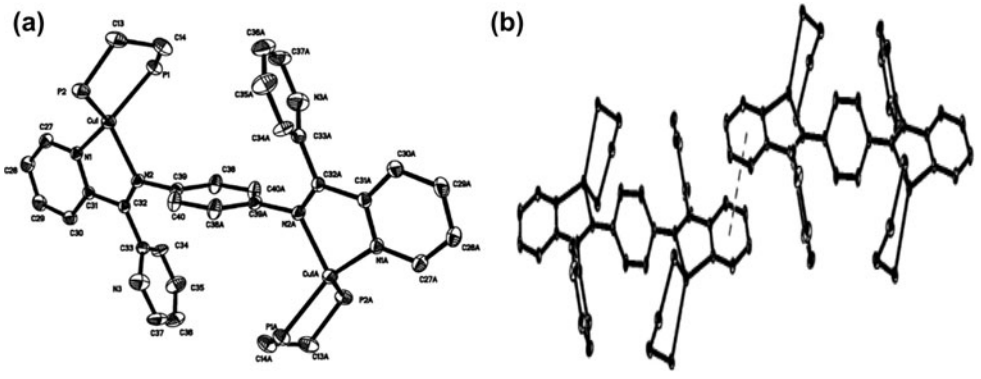

Figure 6. (a) Cation structure of **3**. (b) Intermolecular $\pi\cdots\pi$ stacking interactions between two molecules. The hydrogens and phenyl rings of dppe are deleted for clarity.

Table 5. Hydrogen-bond geometry of **3** (Å, °).

D–H···*A*	*D*–H	H···*A*	*D*···*A*	*D*–H···*A*
C(25)–H(25)···Cg1^{i}	0.93	2.68	3.61	173
C(35)–H(35)···Cg2^{ii}	0.93	2.85	3.71	154
C(40)–H(40)···Cg3^{iii}	0.93	2.74	3.46	135
C(10)–H(10)···O(3)^{iv}	0.93	2.46	3.28	147

Symmetry codes: (i) $1/2-x, 1/2+y, 1/2-z$; (ii) $x, -1+y, z$; (iii) x, y, z; (iv) $-1/2+x, 3/2-y, -1/2+z$. The Cg1, Cg2 are the centroids of the N1–C27–C28–C29–C30–C31, and C7–12 rings, respectively.

Table 6. HOMO, LUMO energy (eV), and energy gap (eV) of $[Cu_2(L)(dppe)_2]^{2+}$ (**1a**) and $[Cu_2(L)(dppp)_2]^{2+}$ (**2a**).

	HOMO (eV)	LUMO (eV)	Energy gap (eV)
$[Cu_2(L)(dppe)_2]^{2+}$ (**1a**)	−6.31	−5.02	1.29
$[Cu_2(L)(dppp)_2]^{2+}$ (**2a**)	−5.81	−4.41	1.40

3.3. *DFT studied*

$[Cu_2(L)(dppe)_2]^{2+}$ (**1a**) and $[Cu_2(L)(dppp)_2]^{2+}$ (**2a**) have potential for metal-centered oxidation in **1** and **2**, comparable with those in similar compounds [46]. Thus, only quantum chemical calculations for **1a** and **2a** were carried out. The main compositions of the HOMO, LUMO, and energy gaps for **1a** and **2a** are ruled out in table 6. The HOMO → LUMO excitation of **1a** is calculated at 1.29 eV, decreasing the HOMO → LUMO energy gap (0.11 eV) in comparison to that of **2a** (1.40 eV). One would expect the energy gaps (ΔE) to decrease in the order **2a** > **1a**. Due to metal-centered oxidation process is mainly related to the cations, the energy gaps of **2** may increase in comparison to that of **1**.

3.4. *Spectroscopic properties*

X-ray diffraction analysis displays that **1** and **3** are isostructural; only the details of **1** are discussed here. The optical properties of **1** and **2** in acetonitrile at room temperature are shown in figure 7. All the complexes have the highest energy bands from 200–300 nm with a molar extinction coefficient (ε) of 10,000–60,000 M^{-1} cm^{-1}, which are assigned as intraligand $\pi \rightarrow \pi^*$ transitions [47]. The lowest energy bands for **1** and **2** have the same peak near 450 nm ($\varepsilon \approx 7200$ M^{-1} cm^{-1}), which is assigned to metal-to-ligand charge transfer (MLCT) absorption whose magnitude of the extinction coefficient is on the order expected for dπ–π^* transitions [48], revealing limited dependence on the identity of the phosphine ligands.

Complexes **1** and **2** are photoluminescent in acetonitrile at room temperature. Complex **1**, upon excitation at 495 nm, exhibits emission with a λ_{max} at 577 nm at room temperature, while **2** shows emission λ_{max} at 572 nm upon excitation at 491 nm. Due to the ligands being not photoluminescent above 500 nm, the emissions of **1** and **2** are assigned to MLCT excited states [49]. In addition, the emission spectra of **1** and **2** reveal a broad orange-red emission band at room temperature with excitation at 435 nm [figure 8(a)]. The emission

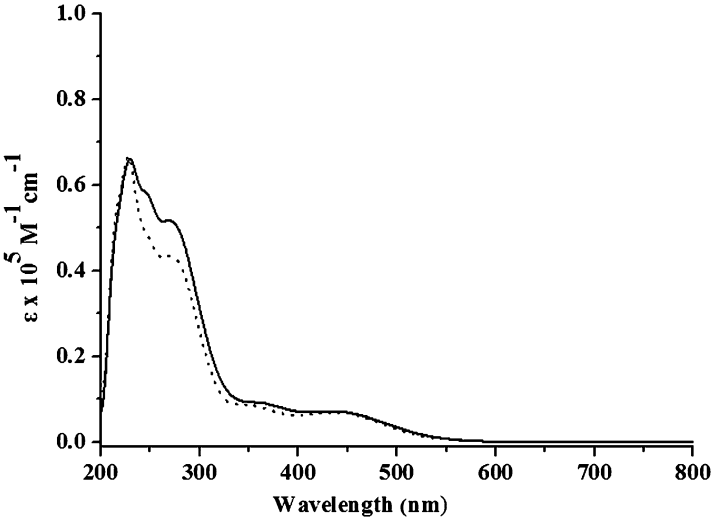

Figure 7. UV–vis absorption spectra of **1** (—) and **2** (···) in CH_3CN (5×10^{-5} M) at room temperature.

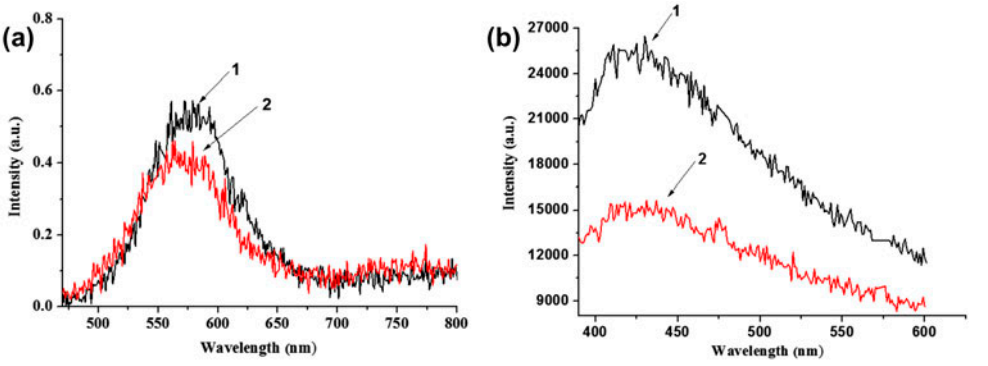

Figure 8. (a) Emission spectra of **1** (black) and **2** (red) in acetonitrile solution (5×10^{-4} M) at room temperature, upon excitation at 435 nm; (b) Solid-state emission spectra of **1** (black) and **2** (red) at room temperature, upon excitation at 350 nm (see http://dx.doi.org/10.1080/00958972.2015.1025770 for color version).

spectra of **1** and **2** are recorded at 570 and 566 nm. As a result, the emission spectrum of **1** in acetonitrile solution is red-shift 4 nm compared to **2**.

Solid-state emissions of **1** and **2** reveal that bridging dppp instead of dppe does not significantly affect the photophysical properties of these complexes [figure 8(b)]. Emission profiles are broad with maxima at 410–450 nm, not similar to those of solution samples [figure 8(a) and (b)]. The emission spectra of **1** and **2** are recorded at 437 and 438 nm, which may be tentatively assigned to MLCT.

3.5. *DSSC performance*

The performance of $[Cu_2(L)(dppe)_2](BF_4)_2$ (**1**) and $[Cu_2(L)(dppp)_2](BF_4)_2{\cdot}2CH_3CN$ (**2**) in a DSSC was studied. Cells were prepared following overnight dyeing of the TiO_2 films from a 0.5 mmol acetonitrile solution of the dye. Table 7 summarizes the DSSC characteristics measured for each cell and with respect to the Ru(II)-based dye N719. All cells were masked to prevent overestimation of conversion efficiency. In the surface-bound heteroleptic dyes **1** and **2**, there are little change to the short circuit current density (J_{SC}) and fill factor (FF) for each cell, but the open circuit voltage and absolute efficiencies are lower for **2** than for **1** [figure 9 and table 7]. Similar to the previous report for other Cu(I)-based dyes [11, 50], overall efficiencies of **1** and **2** as sensitizers in DSSC were poor. All these show that the cell efficiencies are slightly improved by the change in the size of phosphine ligands. The reason for this is due to less efficient electron injection into the TiO_2

Table 7. DSSC performance data for N719, **1** and **2**.

Cell (dye)	J_{SC} (mA cm^{-2})	V_{OC} (mV)	FF	η (%)
1	0.16	445	0.41	0.03
2	0.19	296	0.37	0.02
N719	6.43	782	0.61	3.05

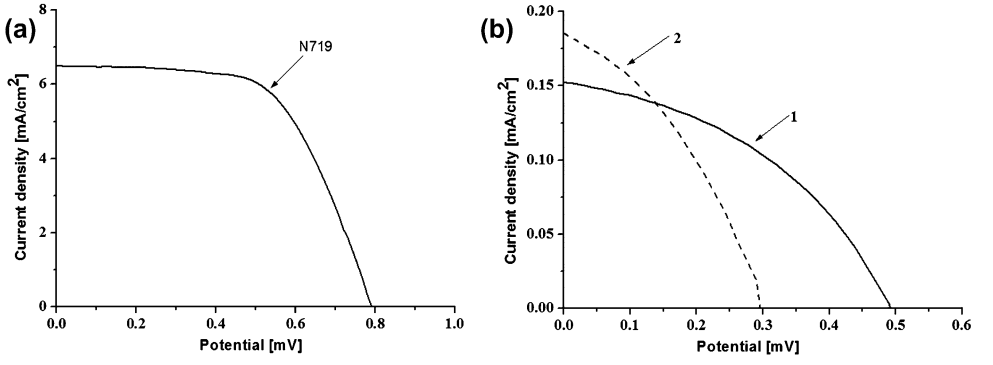

Figure 9. Current density (J_{SC}) against open-circuit voltage (V_{OC}) curves for N719 (a), **1** and **2** (b).

conduction band without the need to isolate the acid complexes, also reflected in comparing conversion efficiency of the dyes **1** and **2** ($\eta_1 = 0.03\%$ and $\eta_2 = 0.02\%$) and standard dye N719 ($\eta = 3.05\%$), as shown in table 7.

4. Conclusion

Three new Cu^+ complexes with N,N′-bis(dipyridin-2-ylmethylene)benzene-1,4-diamine (L) and dppe or dppp have been synthesized and characterized. X-ray diffraction measurement shows L takes a *trans* coordination mode to link two Cu^+ ions, each of which is four-coordinate to form a distorted tetrahedron composed of two P from one phosphine ligand and two N from L. For **1**, **2,** and **3**, intermolecular π-stacking interactions aggregate into cyclic 1-D arrays and the ordered-layer-lattice BF_4^- or CH_3CN is located between these arrays. The optical properties and luminescent properties of **1** and **2** at room temperature are characterized by broad MLCT bands. Complexes **1** and **2** have also been used to prepare DSSC, and the highest energy conversion efficiencies observed for **1** and **2** ($\eta = 0.03$ and 0.02% compared to 3.05% for standard dye N719).

Supplemental material

Crystallographic data for **1**, **2,** and **3** have been deposited with the Cambridge Crystallographic Data Center (CCDC 949849, 949850 and 949851). Copies of the data can be obtained, free of charge, on application to CCDC, 12 Union Road, Cambridge CB2 1EZ, UK; E-mail: deposit@ccdc.cam.ac.uk; or www: http://www.ccdc.cam.ac.uk/deposit.

Disclosure statement

No potential conflict of interest was reported by the authors.

Funding

This work was financially sponsored by the Talent Introduction Funds of Sichuan University of Science and Engineering [grant number 2014RC29]; Key Project of Sichuan Education Department [grant number 15ZA0223].

References

[1] Y.-J. Li, Z.-Y. Deng, X.-F. Xu, H.-B. Wu, Z.-X. Cao, Q.-M. Wang. *Chem. Commun.*, **47**, 9179 (2011).
[2] C.E. McCusker, F.N. Castellano. *Chem. Commun.*, **49**, 3537 (2013).
[3] M.J. Leitl, V.A. Krylova, P.I. Djurovich, M.E. Thompson, H. Yersin. *J. Am. Chem. Soc.*, **136**, 16032 (2014).
[4] D. Volz, M. Wallesch, S.L. Grage, J. Göttlicher, R. Steininger, D. Batchelor, T. Vitova, A.S. Ulrich, C. Heske, L. Weinhardt, T. Baumann, S. Bräse. *Inorg. Chem.*, **53**, 7837 (2014).
[5] X.-L. Xin, M. Chen, Y.-B. Ai, F.-L. Yang, X.-L. Li, F. Li. *Inorg. Chem.*, **53**, 2922 (2014).
[6] D.M. Zink, D. Volz, T. Baumann, M. Mydlak, H. Flügge, J. Friedrichs, M. Nieger, S. Bräse. *Chem. Mater.*, **25**, 4471 (2013).
[7] T. Bessho, E.C. Constable, M. Graetzel, A. Hernandez Redondo, C.E. Housecroft, W. Kylberg, M.K. Nazeeruddin, M. Neuburger, S. Schaffner. *Chem. Commun.*, 3717 (2008).
[8] B. Bozic-Weber, V. Chaurin, E.C. Constable, C.E. Housecroft, M. Meuwly, M. Neuburger, J.A. Rudd, E. Schonhofer, L. Siegfried. *Dalton Trans.*, **41**, 14157 (2012).
[9] B. Bozic-Weber, S.Y. Brauchli, E.C. Constable, S.O. Furer, C.E. Housecroft, I.A. Wright. *Phys. Chem. Chem. Phys.*, **15**, 4500 (2013).
[10] S.Y. Brauchli, B. Bozic-Weber, E.C. Constable, N. Hostettler, C.E. Housecroft, J.A. Zampese. *RSC Adv.*, **4**, 34801 (2014).
[11] T.E. Hewat, L.J. Yellowlees, N. Robertson. *Dalton Trans.*, **43**, 4127 (2014).
[12] N. Armaroli. *Chem. Soc. Rev.*, **30**, 113 (2001).
[13] L. Alibabaei, M. Wang, R. Giovannetti, J. Teuscher, D. Di Censo, J.-E. Moser, P. Comte, F. Pucciarelli, S.M. Zakeeruddin, M. Gratzel. *Energy Environ. Sci.*, **3**, 956 (2010).
[14] C.L. Linfoot, P. Richardson, T.E. Hewat, O. Moudam, M.M. Forde, A. Collins, F. White, N. Robertson. *Dalton Trans.*, **39**, 8945 (2010).
[15] C. Bizzarri, C. Strabler, J. Prock, B. Trettenbrein, M. Ruggenthaler, C.-H. Yang, F. Polo, A. Iordache, P. Brueggeler, L. De Cola. *Inorg. Chem.*, **53**, 10944 (2014).
[16] M. Yu, T.I. Draskovic, Y. Wu. *Phys. Chem. Chem. Phys.*, **16**, 5026 (2014).
[17] Y. Zhao, Y. Zhang, Y. Li, Z. He, Z. Yan. *RSC Adv.*, **2**, 11544 (2012).
[18] R. Hou, T.-H. Huang, X.-J. Wang, X.-F. Jiang, Q.-L. Ni, L.-C. Gui, Y.-J. Fan, Y.-L. Tan. *Dalton Trans.*, **40**, 7551 (2011).
[19] T.-H. Huang, M.-H. Zhang. *Inorg. Chim. Acta*, **416**, 28 (2014).
[20] T.-H. Huang, M.-H. Zhang. *Inorg. Chim. Acta*, **410**, 150 (2014).
[21] Q.-L. Ni, X.-F. Jiang, L.-C. Gui, X.-J. Wang, K.-G. Yang, X.-S. Bi. *New J. Chem.*, **35**, 2471 (2011).
[22] B.L. Booth, K.-S. Li, C.A. McAuliffe. *J. Chem. Soc., Dalton Trans.*, 2959 (1987).
[23] N. Janjic, G. Peli, L. Garlaschelli, A. Sironi, P. Macchi. *Cryst. Growth Des.*, **8**, 854 (2008).
[24] M.W. Jones, G. Mantovani, S.M. Ryan, X. Wang, D.J. Brayden, D.M. Haddleton. *Chem. Commun.*, 5272 (2009).
[25] Z.-W. Tan, C.-Y. Wu, M. Zhang, W.-Z. Lv, J.-J. Qiu, C.-M. Liu. *RSC Adv.*, **4**, 41705 (2014).
[26] T. Mathieson, A. Schier, H. Schmidbaur. *J. Chem. Soc., Dalton Trans.*, 1196 (2001).
[27] B.-C. Tzeng, W.-C. Lo, C.-M. Che, S.-M. Peng. *Chem. Commun.*, 181 (1996).
[28] I.O. Koshevoy, A.J. Karttunen, I.S. Kritchenkou, D.V. Krupenya, S.I. Selivanov, A.S. Melnikov, S.P. Tunik, M. Haukka, T.A. Pakkanen. *Inorg. Chem.*, **52**, 3663 (2013).
[29] S.Y.-L. Leung, W.H. Lam, N. Zhu, V.W.-W. Yam. *Organometallics*, **29**, 5558 (2010).
[30] A. Mangalum, R.C. Smith. *Dalton Trans.*, **39**, 5145 (2010).
[31] J.R. Shakirova, E.V. Grachova, V.V. Gurzhiy, I.O. Koshevoy, A.S. Melnikov, O.V. Sizova, S.P. Tunik, A. Laguna. *Dalton Trans.*, **41**, 2941 (2012).
[32] J.-F. Zhang, W.-F. Fu, X. Gan, J.-H. Chen. *Dalton Trans.*, 3093 (2008).
[33] A. Kaeser, M. Mohankumar, J. Mohanraj, F. Monti, M. Holler, J.-J. Cid, O. Moudam, I. Nierengarten, L. Karmazin-Brelot, C. Duhayon, B. Delavaux-Nicot, N. Armaroli, J.-F. Nierengarten. *Inorg. Chem.*, **52**, 12140 (2013).
[34] J. Min, Q. Zhang, W. Sun, Y. Cheng, L. Wang. *Dalton Trans.*, **40**, 686 (2011).
[35] L. Qin, Q. Zhang, W. Sun, J. Wang, C. Lu, Y. Cheng, L. Wang. *Dalton Trans.*, 9388 (2009).
[36] X.-J. Wang, L.-C. Gui, Q.-L. Ni, Y.-F. Liao, X.-F. Jiang, L.-H. Tang, Z. Zhang, Q. Wu. *CrystEngComm*, **10**, 1003 (2008).
[37] S. Burattini, B.W. Greenland, D.H. Merino, W. Weng, J. Seppala, H.M. Colquhoun, W. Hayes, M.E. Mackay, I.W. Hamley, S.J. Rowan. *J. Am. Chem. Soc.*, **132**, 12051 (2010).

[38] L.J. Childs, N.W. Alcock, M.J. Hannon. *Angew. Chem. Int. Ed.*, **40**, 1079 (2001).
[39] D.L. Reger, A. Debreczeni, M.D. Smith, J. Jezierska, A. Ozarowski. *Inorg. Chem.*, **51**, 1068 (2011).
[40] P.J. Ball, T.R. Shtoyko, J.A. Krause Bauer, W.J. Oldham, W.B. Connick. *Inorg. Chem.*, **43**, 622 (2003).
[41] J.D.A. Pelletier, J. Fawcett, K. Singh, G.A. Solan. *J. Organomet. Chem.*, **693**, 2723 (2008).
[42] D. Tzimopoulos, A. Czapik, S. Kotoulas, J. Mohanraj, M. Gdaniec, P.D. Akrivos. *J. Coord. Chem.*, **65**, 393 (2012).
[43] X. Liu, H. Nan, W. Sun, Q. Zhang, M. Zhan, L. Zou, Z. Xie, X. Li, C. Lu, Y. Cheng. *Dalton Trans.*, **41**, 10199 (2012).
[44] J.-J. Cid, J. Mohanraj, M. Mohankumar, M. Holler, G. Accorsi, L. Brelot, I. Nierengarten, O. Moudam, A. Kaeser, B. Delavaux-Nicot, N. Armaroli, J.-F. Nierengarten. *Chem. Commun.*, **49**, 859 (2013).
[45] C. Femoni, S. Muzzioli, A. Palazzi, S. Stagni, S. Zacchini, F. Monti, G. Accorsi, M. Bolognesi, N. Armaroli, M. Massi, G. Valenti, M. Marcaccio. *Dalton Trans.*, **42**, 997 (2013).
[46] B. Bozic-Weber, S.Y. Brauchli, E.C. Constable, S.O. Furer, C.E. Housecroft, F.J. Malzner, I.A. Wright, J.A. Zampese. *Dalton Trans.*, **42**, 12293 (2013).
[47] G.F. Manbeck, W.W. Brennessel, R. Eisenberg. *Inorg. Chem.*, **50**, 3431 (2011).
[48] D.M. Zink, M. Bächle, T. Baumann, M. Nieger, M. Kühn, C. Wang, W. Klopper, U. Monkowius, T. Hofbeck, H. Yersin, S. Bräse. *Inorg. Chem.*, **52**, 2292 (2012).
[49] M.G. Crestani, G.F. Manbeck, W.W. Brennessel, T.M. McCormick, R. Eisenberg. *Inorg. Chem.*, **50**, 7172 (2011).
[50] M. Sandroni, M. Kayanuma, A. Planchat, N. Szuwarski, E. Blart, Y. Pellegrin, C. Daniel, M. Boujtita, F. Odobel. *Dalton Trans.*, **42**, 10818 (2013).